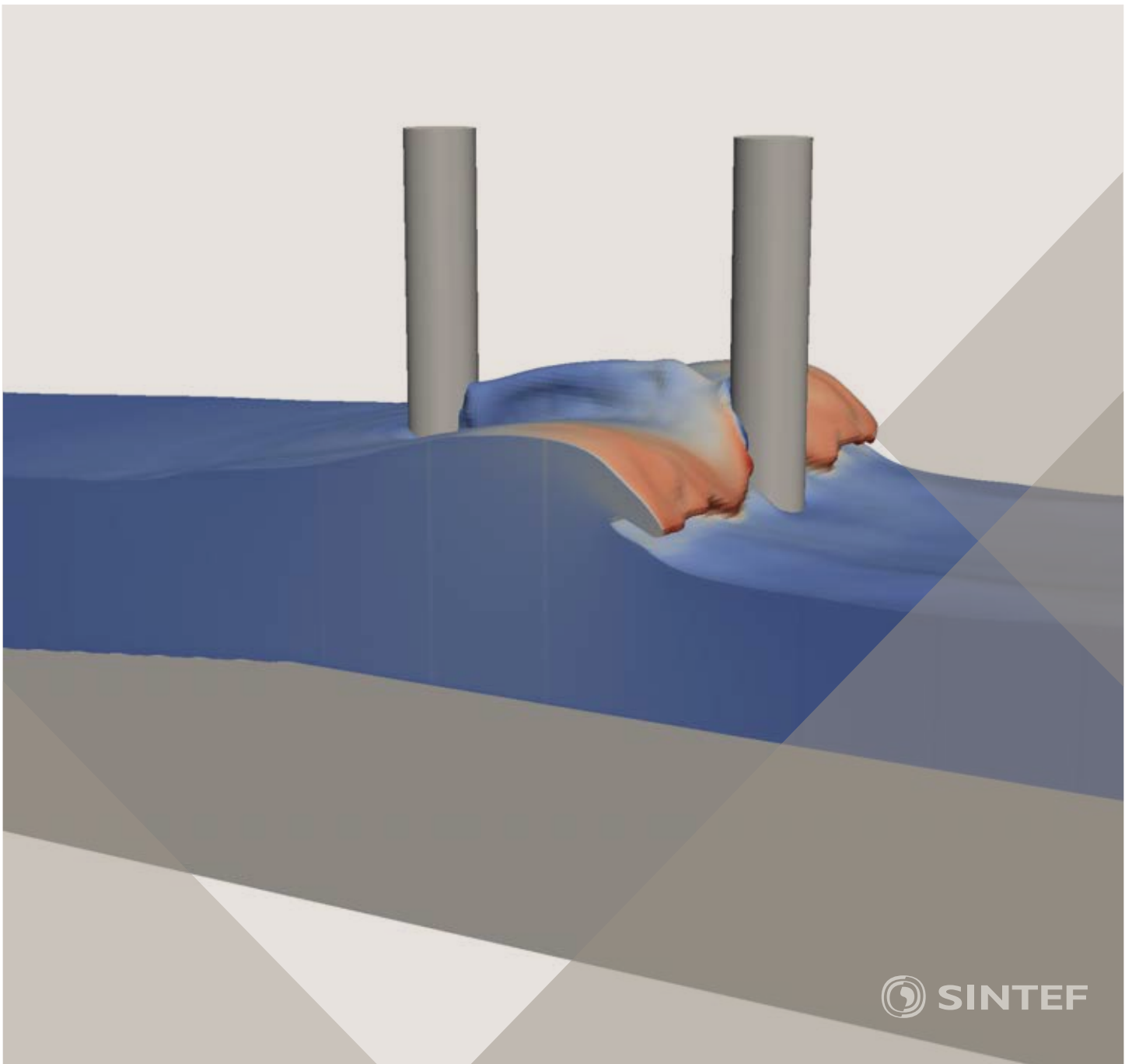


Proceedings of the 12<sup>th</sup> International Conference on  
Computational Fluid Dynamics in the Oil & Gas,  
Metallurgical and Process Industries

# Progress in Applied CFD – CFD2017



SINTEF Proceedings

Editors:

Jan Erik Olsen and Stein Tore Johansen

## **Progress in Applied CFD – CFD2017**

Proceedings of the 12<sup>th</sup> International Conference on Computational Fluid Dynamics  
in the Oil & Gas, Metallurgical and Process Industries

SINTEF Academic Press

SINTEF Proceedings no 2

Editors: Jan Erik Olsen and Stein Tore Johansen

**Progress in Applied CFD – CFD2017**

Selected papers from 10<sup>th</sup> International Conference on Computational Fluid Dynamics in the Oil & Gas, Metallurgical and Process Industries

Key words:

CFD, Flow, Modelling

Cover, illustration: Arun Kamath

ISSN 2387-4295 (online)

ISBN 978-82-536-1544-8 (pdf)

© Copyright SINTEF Academic Press 2017

The material in this publication is covered by the provisions of the Norwegian Copyright Act. Without any special agreement with SINTEF Academic Press, any copying and making available of the material is only allowed to the extent that this is permitted by law or allowed through an agreement with Kopinor, the Reproduction Rights Organisation for Norway. Any use contrary to legislation or an agreement may lead to a liability for damages and confiscation, and may be punished by fines or imprisonment

SINTEF Academic Press

Address:       Forskningsveien 3 B  
                  PO Box 124 Blindern  
                  N-0314 OSLO

Tel:             +47 73 59 30 00

Fax:            +47 22 96 55 08

[www.sintef.no/byggforsk](http://www.sintef.no/byggforsk)

[www.sintefbok.no](http://www.sintefbok.no)

**SINTEF Proceedings**

SINTEF Proceedings is a serial publication for peer-reviewed conference proceedings on a variety of scientific topics.

The processes of peer-reviewing of papers published in SINTEF Proceedings are administered by the conference organizers and proceedings editors. Detailed procedures will vary according to custom and practice in each scientific community.

## PREFACE

This book contains all manuscripts approved by the reviewers and the organizing committee of the 12th International Conference on Computational Fluid Dynamics in the Oil & Gas, Metallurgical and Process Industries. The conference was hosted by SINTEF in Trondheim in May/June 2017 and is also known as CFD2017 for short. The conference series was initiated by CSIRO and Phil Schwarz in 1997. So far the conference has been alternating between CSIRO in Melbourne and SINTEF in Trondheim. The conferences focuses on the application of CFD in the oil and gas industries, metal production, mineral processing, power generation, chemicals and other process industries. In addition pragmatic modelling concepts and bio-mechanical applications have become an important part of the conference. The papers in this book demonstrate the current progress in applied CFD.

The conference papers undergo a review process involving two experts. Only papers accepted by the reviewers are included in the proceedings. 108 contributions were presented at the conference together with six keynote presentations. A majority of these contributions are presented by their manuscript in this collection (a few were granted to present without an accompanying manuscript).

The organizing committee would like to thank everyone who has helped with review of manuscripts, all those who helped to promote the conference and all authors who have submitted scientific contributions. We are also grateful for the support from the conference sponsors: ANSYS, SFI Metal Production and NanoSim.

Stein Tore Johansen & Jan Erik Olsen



Organizing committee:

Conference chairman: Prof. Stein Tore Johansen

Conference coordinator: Dr. Jan Erik Olsen

Dr. Bernhard Müller

Dr. Sigrid Karstad Dahl

Dr. Shahriar Amini

Dr. Ernst Meese

Dr. Josip Zoric

Dr. Jannike Solsvik

Dr. Peter Witt

Scientific committee:

Stein Tore Johansen, SINTEF/NTNU

Bernhard Müller, NTNU

Phil Schwarz, CSIRO

Akio Tomiyama, Kobe University

Hans Kuipers, Eindhoven University of Technology

Jinghai Li, Chinese Academy of Science

Markus Braun, Ansys

Simon Lo, CD-adapco

Patrick Segers, Universiteit Gent

Jiyuan Tu, RMIT

Jos Derksen, University of Aberdeen

Dmitry Eskin, Schlumberger-Doll Research

Pär Jönsson, KTH

Stefan Pirker, Johannes Kepler University

Josip Zoric, SINTEF

# CONTENTS

<b>PRAGMATIC MODELLING .....</b>	<b>9</b>
On pragmatism in industrial modeling. Part III: Application to operational drilling .....	11
CFD modeling of dynamic emulsion stability .....	23
Modelling of interaction between turbines and terrain wakes using pragmatic approach .....	29
<b>FLUIDIZED BED .....</b>	<b>37</b>
Simulation of chemical looping combustion process in a double looping fluidized bed reactor with cu-based oxygen carriers.....	39
Extremely fast simulations of heat transfer in fluidized beds.....	47
Mass transfer phenomena in fluidized beds with horizontally immersed membranes .....	53
A Two-Fluid model study of hydrogen production via water gas shift in fluidized bed membrane reactors .....	63
Effect of lift force on dense gas-fluidized beds of non-spherical particles .....	71
Experimental and numerical investigation of a bubbling dense gas-solid fluidized bed .....	81
Direct numerical simulation of the effective drag in gas-liquid-solid systems .....	89
A Lagrangian-Eulerian hybrid model for the simulation of direct reduction of iron ore in fluidized beds.....	97
High temperature fluidization - influence of inter-particle forces on fluidization behavior .....	107
Verification of filtered two fluid models for reactive gas-solid flows .....	115
<b>BIOMECHANICS.....</b>	<b>123</b>
A computational framework involving CFD and data mining tools for analyzing disease in carotid artery .....	125
Investigating the numerical parameter space for a stenosed patient-specific internal carotid artery model.....	133
Velocity profiles in a 2D model of the left ventricular outflow tract, pathological case study using PIV and CFD modeling.....	139
Oscillatory flow and mass transport in a coronary artery.....	147
Patient specific numerical simulation of flow in the human upper airways for assessing the effect of nasal surgery.....	153
CFD simulations of turbulent flow in the human upper airways .....	163
<b>OIL &amp; GAS APPLICATIONS .....</b>	<b>169</b>
Estimation of flow rates and parameters in two-phase stratified and slug flow by an ensemble Kalman filter .....	171
Direct numerical simulation of proppant transport in a narrow channel for hydraulic fracturing application .....	179
Multiphase direct numerical simulations (DNS) of oil-water flows through homogeneous porous rocks .....	185
CFD erosion modelling of blind tees .....	191
Shape factors inclusion in a one-dimensional, transient two-fluid model for stratified and slug flow simulations in pipes .....	201
Gas-liquid two-phase flow behavior in terrain-inclined pipelines for wet natural gas transportation .....	207

<b>NUMERICS, METHODS &amp; CODE DEVELOPMENT .....</b>	<b>213</b>
Innovative computing for industrially-relevant multiphase flows .....	215
Development of GPU parallel multiphase flow solver for turbulent slurry flows in cyclone.....	223
Immersed boundary method for the compressible Navier–Stokes equations using high order summation-by-parts difference operators .....	233
Direct numerical simulation of coupled heat and mass transfer in fluid-solid systems .....	243
A simulation concept for generic simulation of multi-material flow, using staggered Cartesian grids.....	253
A cartesian cut-cell method, based on formal volume averaging of mass, momentum equations.....	265
SOFT: a framework for semantic interoperability of scientific software .....	273
<b>POPULATION BALANCE .....</b>	<b>279</b>
Combined multifluid-population balance method for polydisperse multiphase flows .....	281
A multifluid-PBE model for a slurry bubble column with bubble size dependent velocity, weight fractions and temperature.....	285
CFD simulation of the droplet size distribution of liquid-liquid emulsions in stirred tank reactors .....	295
Towards a CFD model for boiling flows: validation of QMOM predictions with TOPFLOW experiments .....	301
Numerical simulations of turbulent liquid-liquid dispersions with quadrature-based moment methods.....	309
Simulation of dispersion of immiscible fluids in a turbulent couette flow .....	317
Simulation of gas-liquid flows in separators - a Lagrangian approach.....	325
CFD modelling to predict mass transfer in pulsed sieve plate extraction columns .....	335
<b>BREAKUP &amp; COALESCENCE .....</b>	<b>343</b>
Experimental and numerical study on single droplet breakage in turbulent flow .....	345
Improved collision modelling for liquid metal droplets in a copper slag cleaning process .....	355
Modelling of bubble dynamics in slag during its hot stage engineering.....	365
Controlled coalescence with local front reconstruction method .....	373
<b>BUBBLY FLOWS .....</b>	<b>381</b>
Modelling of fluid dynamics, mass transfer and chemical reaction in bubbly flows .....	383
Stochastic DSMC model for large scale dense bubbly flows.....	391
On the surfacing mechanism of bubble plumes from subsea gas release.....	399
Bubble generated turbulence in two fluid simulation of bubbly flow .....	405
<b>HEAT TRANSFER .....</b>	<b>413</b>
CFD-simulation of boiling in a heated pipe including flow pattern transitions using a multi-field concept .....	415
The pear-shaped fate of an ice melting front .....	423
Flow dynamics studies for flexible operation of continuous casters (flow flex cc).....	431
An Euler-Euler model for gas-liquid flows in a coil wound heat exchanger.....	441
<b>NON-NEWTONIAN FLOWS.....</b>	<b>449</b>
Viscoelastic flow simulations in disordered porous media .....	451
Tire rubber extrudate swell simulation and verification with experiments .....	459
Front-tracking simulations of bubbles rising in non-Newtonian fluids.....	469
A 2D sediment bed morphodynamics model for turbulent, non-Newtonian, particle-loaded flows.....	479

<b>METALLURGICAL APPLICATIONS.....</b>	<b>491</b>
Experimental modelling of metallurgical processes .....	493
State of the art: macroscopic modelling approaches for the description of multiphysics phenomena within the electroslag remelting process .....	499
LES-VOF simulation of turbulent interfacial flow in the continuous casting mold .....	507
CFD-DEM modelling of blast furnace tapping .....	515
Multiphase flow modelling of furnace tapholes .....	521
Numerical predictions of the shape and size of the raceway zone in a blast furnace.....	531
Modelling and measurements in the aluminium industry - Where are the obstacles? .....	541
Modelling of chemical reactions in metallurgical processes.....	549
Using CFD analysis to optimise top submerged lance furnace geometries .....	555
Numerical analysis of the temperature distribution in a martensitic stainless steel strip during hardening.....	565
Validation of a rapid slag viscosity measurement by CFD.....	575
Solidification modeling with user defined function in ANSYS Fluent.....	583
Cleaning of polycyclic aromatic hydrocarbons (PAH) obtained from ferroalloys plant.....	587
Granular flow described by fictitious fluids: a suitable methodology for process simulations .....	593
A multiscale numerical approach of the dripping slag in the coke bed zone of a pilot scale Si-Mn furnace.....	599
<b>INDUSTRIAL APPLICATIONS .....</b>	<b>605</b>
Use of CFD as a design tool for a phosphoric acid plant cooling pond .....	607
Numerical evaluation of co-firing solid recovered fuel with petroleum coke in a cement rotary kiln: Influence of fuel moisture .....	613
Experimental and CFD investigation of fractal distributor on a novel plate and frame ion-exchanger .....	621
<b>COMBUSTION .....</b>	<b>631</b>
CFD modeling of a commercial-size circle-draft biomass gasifier.....	633
Numerical study of coal particle gasification up to Reynolds numbers of 1000.....	641
Modelling combustion of pulverized coal and alternative carbon materials in the blast furnace raceway .....	647
Combustion chamber scaling for energy recovery from furnace process gas: waste to value .....	657
<b>PACKED BED.....</b>	<b>665</b>
Comparison of particle-resolved direct numerical simulation and 1D modelling of catalytic reactions in a packed bed .....	667
Numerical investigation of particle types influence on packed bed adsorber behaviour .....	675
CFD based study of dense medium drum separation processes .....	683
A multi-domain 1D particle-reactor model for packed bed reactor applications.....	689
<b>SPECIES TRANSPORT &amp; INTERFACES .....</b>	<b>699</b>
Modelling and numerical simulation of surface active species transport - reaction in welding processes .....	701
Multiscale approach to fully resolved boundary layers using adaptive grids.....	709
Implementation, demonstration and validation of a user-defined wall function for direct precipitation fouling in Ansys Fluent.....	717

<b>FREE SURFACE FLOW &amp; WAVES .....</b>	<b>727</b>
Unresolved CFD-DEM in environmental engineering: submarine slope stability and other applications.....	729
Influence of the upstream cylinder and wave breaking point on the breaking wave forces on the downstream cylinder .....	735
Recent developments for the computation of the necessary submergence of pump intakes with free surfaces .....	743
Parallel multiphase flow software for solving the Navier-Stokes equations .....	752
 <b>PARTICLE METHODS .....</b>	 <b>759</b>
A numerical approach to model aggregate restructuring in shear flow using DEM in Lattice-Boltzmann simulations .....	761
Adaptive coarse-graining for large-scale DEM simulations.....	773
Novel efficient hybrid-DEM collision integration scheme.....	779
Implementing the kinetic theory of granular flows into the Lagrangian dense discrete phase model.....	785
Importance of the different fluid forces on particle dispersion in fluid phase resonance mixers .....	791
Large scale modelling of bubble formation and growth in a supersaturated liquid.....	798
 <b>FUNDAMENTAL FLUID DYNAMICS .....</b>	 <b>807</b>
Flow past a yawed cylinder of finite length using a fictitious domain method .....	809
A numerical evaluation of the effect of the electro-magnetic force on bubble flow in aluminium smelting process.....	819
A DNS study of droplet spreading and penetration on a porous medium.....	825
From linear to nonlinear: Transient growth in confined magnetohydrodynamic flows.....	831



# COMBUSTION CHAMBER SCALING FOR ENERGY RECOVERY FROM FURNACE PROCESS GAS: WASTE TO VALUE

**Balram Panjwani, Bernd Wittgens, and Jan Erik Olsen**

SINTEF Materials and Chemistry, 7465 Trondheim, NORWAY

\* E-mail: balram.panjwani@sintef.no

## ABSTRACT

One of the byproducts during the metal reduction process is energy rich off-gas of which the energy is normally not used. In the present paper, a novel concept for energy recovery from process gas is discussed. The concept is founded on the idea of introducing a combustion chamber in the off-gas section, which will provide an additional degree of freedom for optimizing energy recovery and minimizing Polycyclic Aromatic Hydrocarbon (PAH) and NO<sub>x</sub> concentrations. Design and operation of the combustion chamber depend on many parameters, including the total power capacity of the combustion chamber, residence time for combusting the complex PAH. The design criteria for the combustion chamber have been identified and discussed. The scaling of the combustion chamber based on proposed design criteria is presented. Engineering methods and Computational Fluid Dynamics (CFD) has been utilized extensively for scaling the combustion chamber. The results from our CFD simulations of the flow in the combustion chamber, exploring different off-gas fuel compositions, are presented. In brief, the paper covers all aspects which influences the scaling of the combustion chamber, including insulation thickness, choice of insulating material, heat transfer through extended surfaces, multi-staging and secondary air injection.

**Keywords:** CFD, Combustion chamber, Ferro Alloys, Furnace.

## NOMENCLATURE

A complete list of symbols used, with dimensions, is required.

### Greek Symbols

$\rho$  Mass density, [kg/m<sup>3</sup>].

$\lambda$  Thermal Conductivity,  $\lambda$ , [W/m.s].

### Latin Symbols

$h$  Heat transfer coefficient, [m].

$p$  Pressure, [Pa].

$r_e$  outer radius of the chamber, [m].

$r_i$  inner radius of the chamber, [m].

$r_n$  Radius of nth insulating radius, [m].

### Sub/superscripts

$i$  Index  $i$ .

$j$  Index  $j$ .

## INTRODUCTION

Ferrous alloys is produced in submerged arc furnaces (SAF) where ore and carbon (coke, coal, etc.) are mixed into a charge and allowed to react when electric energy is supplied through electrodes. The reactions produce alloys and an energy rich process gas. The alloys sink to the bottom where it is collected in ladles through a tapping hole. Hot process gas rises upwards through the charge surface into a furnace hood. Simultaneously, in case of open furnace hood, air is sucked into the hood through various open areas due to the pressure drop. The air and process gas reacts inside the hood through a combustion process and produces an off-gas potentially containing CO<sub>2</sub>, H<sub>2</sub>O and other components. This is illustrated in Figure 1. Most of the energy of the process gas is lost due to uncontrolled combustion of CO inside the hood. This is a kind of intriguing system where first energy is supplied to produce a desirable metal and then the energy rich by products are not used. A viable solution to the problem is to recover the energy from the process gas. There are two main potential sources for energy recovery; 1) an off-gas with a high temperature and 2) the cooling water used for cooling the system. An energy analysis carried out by Kamfjord et al. (Kamfjord et al. 2010) has shown utilization of hot water obtained from the furnace for other industries including agriculture, sports etc.

Currently, most of the Si furnaces are open, where use of the energy available in the process gas for electricity production is a challenge. However, in closed furnace the process gas CO does not go through the uncontrolled combustion inside the hood and therefore it is possible to utilize the energy for electricity generation. Heimir Hjartarson et al. (Heimir Hjartarson, Halldor Palsson, and Saevarsdottir 2010) performed an energy and exergy analysis on a 47 MW SAF producing FeSi75 based on measurements. It was concluded that the production of ferrosilicon involves large exergy destruction, estimated to be 46.5 MW, and the exergetic efficiency of the

furnace is about 30%. The energy analysis shows that much of the energy used in the production of ferrosilicon goes into the environment as a waste heat. Only 35.6 MW of the 98 MW of the energy supplied to the process are retrieved as chemical energy in the product.

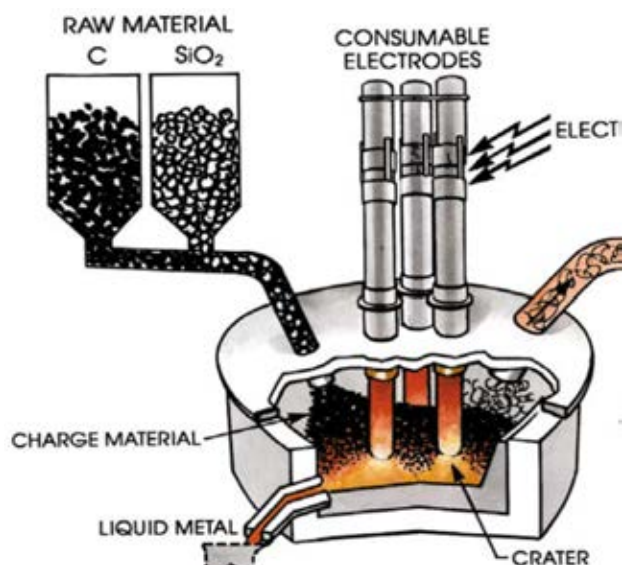


Figure 1: Principle sketch of the metal reduction process. Schei et al (Schei, Tuset, and Tveit 1997)

To obtain energy from the submerged arc furnace, a heat recovery system needs to be designed. One of the principle requirements of a heat recovery system is that it should not affect the quantity and quality of the product and it should not increase primary energy (coal, oil or natural gas) consumption. The heat recovery system should extract energy available in sensible heat of waste hot water and from chemical energy available in flue gas. The recovery system needs to be safe, reliable, sustainable, and stable with a reduced amount of smoke/dust and other pollutant production. The proposed waste heat recovery system is based on the utilization of the chemical energy available in process gas. The system includes a combustion chamber and the primary objective of the proposed combustion chamber is to combust the process gases obtained either from Ferro manganese or from Ferro silicon furnace. The process gas mainly consists of CO, H<sub>2</sub>O, CO<sub>2</sub> and Si component (dust/gas) in Ferro Silicon furnace and Mn components (dust/gas) in Ferromanganese furnace. The process gas also consists of some amount of PAH and oxidation of the PAH is a challenge due to their stable complex rings. One of the objectives of the proposed combustion chamber is to oxidize the PAH. The minimum residence time and temperature to oxidize these PAH rings is around 2s and 800°C respectively (Mati et al. 2007). The other requirement for this combustion chamber is to have better control of the NO<sub>x</sub> formation, which again depends on the temperature and residence time. The peak temperature and simultaneous higher residence time leads to higher NO<sub>x</sub> formation. Thus the two requirements of complete PAH combustion and minimized NO<sub>x</sub> formation are contradictory to each other. However, it is possible to meet both requirements

by having more uniform temperature. Temperature should not exceed the critical temperature responsible for the higher NO<sub>x</sub> formation. The critical temperature for thermal NO<sub>x</sub> formation is above 1500°C. It is possible to optimize the chamber with respect to temperature and residence time. The residence time of the combustion chamber can be calculated either with the Lagrangian approach or with species transport. The Lagrangian approach is computationally demanding and therefore an approach based on species transport is employed. In this approach, an inert species/tracer is released from the process gas inlet. It is assumed that the effect of the tracer on the global flow field is insignificant. Residence time is calculated by solving an unsteady transport equation for the inert species. The concentration of the inert species over time is monitored at the outlet.

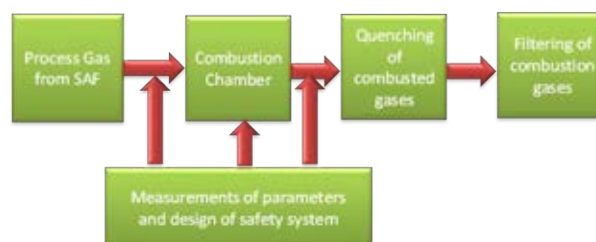


Figure 2: Flow diagram of heat recovery system from flue gas.

An overall concept of the entire system is shown in Figure 2. The objective of the lab-scale plant is only to demonstrate the functioning of the combustion chamber and therefore the current lab-scale plant is not equipped with a power generation system. Process gas from the SAF is transported to the combustion chamber via a suitable connection. Measurements of temperature, species concentration, and other emissions are performed not only downstream and upstream of the combustion chamber, but also inside the combustion chamber. A robust safety system integrated with the measurement system is developed to avoid any accidents. The hot exhaust gases from the combustion chamber are quenched to a suitable temperature before entering into the filter unit.

#### DESIGN CRITERION OF COMBUSTION CHAMBER

The combustion chamber is normally designed considering two different types of flames, either diffusion or premixed. In the diffusion or non-premixed flame, fuel and oxidizer come from a separate stream prior to entering the combustion chamber. However, in the premixed flame, both fuel and oxidizer are mixed prior to entering the combustion chamber. Apart from the type of flames, the combustor performance is also governed by the size and shape of the combustion chamber. Historically, most of the research has been done for the jet engine combustion chamber scaling and therefore most of the design criteria have been laid down for the jet engine combustion chamber. In addition, the existing gas-fired boiler/furnaces design criteria do not meet our requirements and therefore new design criteria are needed to design a combustion chamber to meet our requirements. These are some of the proposed design criteria for scaling the combustion chamber.

1) The combustion chamber has to be based on the pure diffusion flame concept. Operating the combustion chamber with a premixed flame is a challenge due to uncontrolled flame that can affect the furnace safety.

2) Transport of the process gas from the furnace to the combustion chamber requires special attention to avoid any clogging of the pipes due to dust and tar available in the process gas. There are also possibilities of condensation of SiO gas inside the transport pipes and this has to be considered while scaling the transport pipes.

3) The residence time and temperature of the gases inside the combustion chamber should be sufficiently high to achieve a proper mixing and subsequent combustion of PAH.

4) The inner wall temperature of the combustion chamber should not exceed the critical temperature at which the insulating materials have been designed.

5) The maximum temperature on the outer wall of the combustion chamber should not be very high. The outer wall temperature of the combustion chamber shall not exceed 60-100 °C.

7) The temperature of the combusted gases out of the combustion chamber should not be more than 800°C otherwise cooling of the exhaust hot gases will be a challenge.

8) The capacity of the combustion chamber should be around 30 kW. Aim of the combustion chamber was not to produce power but to show an oxidation of PAH and NOx formation. Therefore combustion chamber with small capacity was designed.

9) Last but not least is the price and weight of the whole assembly should not exceed the limit. It is difficult to come with price now and this information is sensitive and could not be shared. It was made sure that pipe size, chamber internal and outer dimension, insulations are of standard dimensions to avoid unnecessary costs.

**COMPUTATIONAL FLUID DYNAMICS (CFD) MODEL OF COMBUSTION CHAMBER**

CFD has been matured enough to be used for designing any industrial or laboratory scale system involving flow, heat and mass transfer. In the present study CFD is utilized for designing and scaling the combustion chamber. All the design parameters discussed earlier have been independently evaluated with CFD. Commercial CFD software ANSYS FLUENT (ANSYS 2016) has been utilized for studies. The geometry and mesh was generated using ANSYS design modeler. The generated mesh was imported into the FLUENT flow solver.

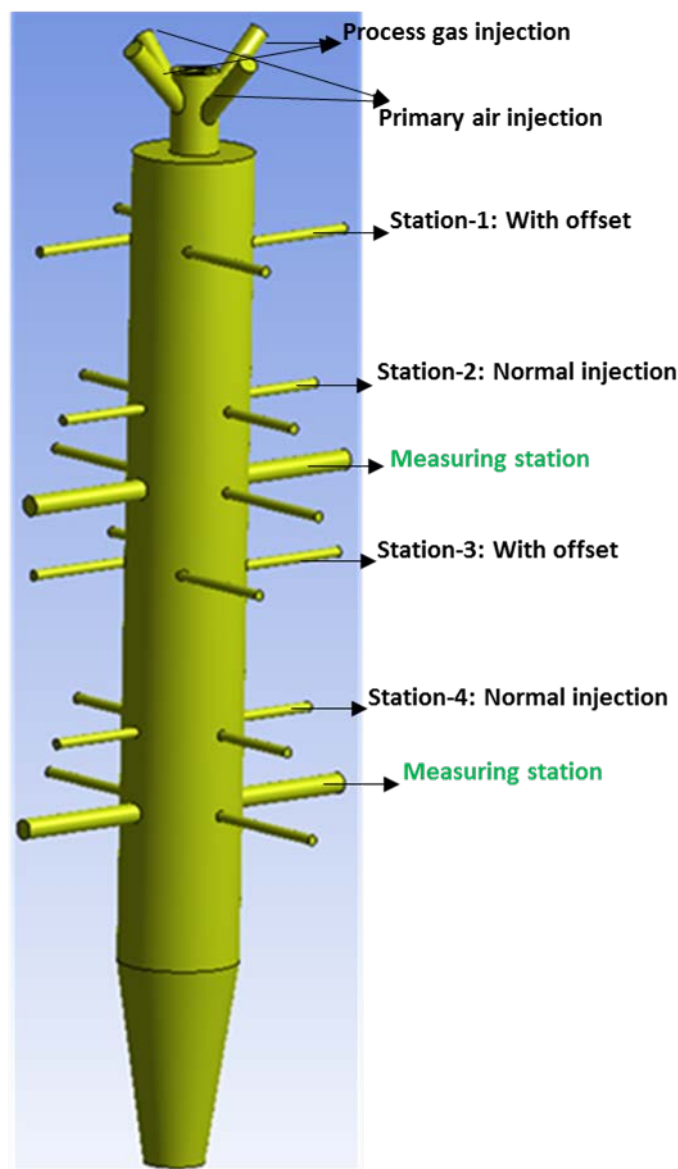


Figure 3: Combustion chamber

In current steady state CFD model setup, the convective and diffusive terms in all the transport equations (mass, momentum, energy, turbulence and species) were discretized using first order accurate scheme during the initial phase of chamber scaling, however, for final scaling, second order scheme was employed. The turbulence-chemistry was modeled with the eddy dissipation concept model. Turbulence was handled with k-e model and for radiation, Discrete Ordinance (DO) model was employed. The process gas mainly consists of 70-75% of CO and 20-25 % of H2O. Oxidation of CO with air was modeled using a detailed chemical kinetic mechanism involving 12 species and 28 elementary reactions (Drake and Blint 1988) as shown in Table-1. The pressure-velocity coupling was achieved by SIMPLE algorithm. Meshing of the geometry was carried out using ANSYS MESH.

Table-1: CO/air mechanism used for present study

```
ELEMENTS
H O C N
END
```

SPECIES

H O2 O OH H2 H2O HO2 CO CO2 HCO H2O2 N2

END

REACTIONS CAL/MOLE

Units are moles, cubic centimeters, and calories per mole. Temperature in Kelvin.

H+O2=O+OH	5.10E+16	-0.816	16507
OH+H2=H2O+H	1.20E+09	1.3	3630
H2+O=H+OH	1.80E+10	1	8920
OH+OH=H2O+O	1.50E+09	1.14	0
H+HO2=OH+OH	1.50E+14	0	1000
H+HO2=H2+O2	2.50E+13	0	690
H+HO2=H2O+O	1.00E+13	0	1073
HO2+OH=H2O+O2	1.50E+13	0	0
HO2+O=O2+OH	2.00E+13	0	0
H2O2+OH=H2O+HO2	1.00E+13	0	1800
HO2+HO2=H2O2+O2	2.00E+12	0	0
H2O2+H=HO2+H2	1.70E+12	0	3750
H+O2+M=HO2+M	2.30E+18	-0.8	0
H2O2+M=OH+OH+M	1.20E+17	0	45500
CO+OH=CO2+H	1.50E+07	1.3	-770
CO+HO2=CO2+OH	1.50E+14	0	23650
CO2+O=CO+O2	2.80E+12	0	43830
HCO+M=H+CO+M	7.10E+14	0	16800
HCO+H=CO+H2	2.00E+14	0	0
HCO+OH=CO+H2O	5.00E+13	0	0
HCO+O2=CO+HO2	5.00E+11	0.5	835
H+H+M=H2+M	9.00E+16	-0.6	0
H+OH+M=H2O+M	2.20E+22	-2	0
O+H+M=OH+M	6.20E+16	-0.6	0
CO+O+M=CO2+M	5.80E+13	0	0
HCO+O=CO+OH	3.00E+13	0	0
HCO+O=CO2+H	3.00E+13	0	0

The model initial mesh was 6.5 million tetrahedral cells, which was converted into polyhedral mesh of 1.8 million cells. The grid was refined close to all walls. In addition, a boundary layer mesh was generated. While converting from tetrahedral mesh to polyhedral mesh, the boundary layer mesh does not change. Global stoichiometric ratio of combustion system is maintain closer to one. Amount of process gas was calculated considering the combustion chamber of 30 kW. The air need for complete combustion is calculated based on the amount of process gas. 20% of air was supplied at the primary air inlet located at the top and remaining 80% of the air was equally distributed into the secondary air inlet. Optimization of stoichiometric ratio through secondary air injection is not performed in the present study.

#### DESIGN CRITERIA FOR COMBUSTION CHAMBER SIZING

The length and diameter of the combustion chamber were based on two parameters initially 1) desired power

capacity of combustor which is around 30 kW and 2) desired residence time require for oxidation of PAH. However, controlling the temperature and residence time only through chamber diameter and length was a challenge; therefore some other parameters/functions on the combustion chamber need to be introduced. The other parameter that can control the residence time inside the combustion chamber could be the arrangement of the air supply. In the combustion chamber, the fuel and oxidizer can be supplied either coaxially or circumferentially. In a coaxial arrangement of fuel and air inlet, the dominating flow direction is along the axis of the combustion chamber and some of the air might travels in a lateral direction due to diffusion. However, in this configuration the residence time is mainly governed by the fuel and air inlet velocities at the coaxial inlet and length of the chamber. Based on our initial finding it was found that the coaxial configuration does not give residence time of 2s necessary for the PAH oxidation. Furthermore, coaxial injection does not provide uniform mixing. The other possibility to improve the residence time is to supply air circumferentially. The air supplied circumferentially is referred here as a secondary air injection. These secondary injections are provided at the offset (see Figure 4) to improve a mixing between fuel and oxidizer.

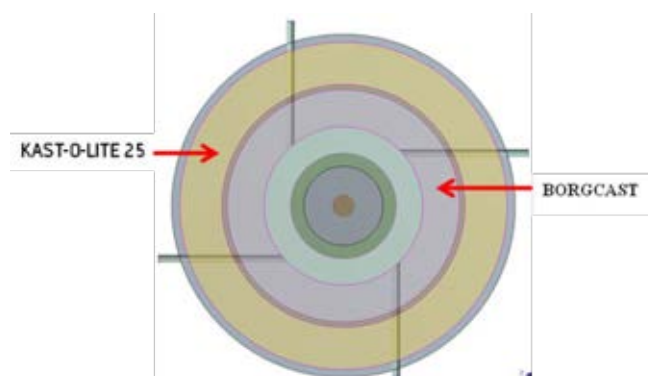


Figure 4: Cross section of the combustion chamber with secondary air injection in offset plane

Figure 4 shows cross section of the combustion chamber with secondary air injection in offset plane. The secondary air was injected at four different locations along the length of the combustion chamber (see Figure 3). At each longitudinal locations four air inlet pipes were provided. In the initial design phase of combustion chamber, all the four pipes were provided circumferentially at offset from the center to obtain the circulation pattern inside the combustion chamber which helps to improve the mixing and subsequent combustion. This arrangement of inlet pipes also increases the residence time of the gases and maintain the gas temperature at lower level, which helps in reduced NOx formation.

However, a challenging problem with this arrangement is a lesser penetration of air deep inside the chamber where most of the process gas is available. This problem was solved by removing offset for the secondary air inlet at second and fourth stations. The offset was only provided at first and second station for secondary air

inlet. The perpendicular locations of air inlet at second and fourth gave deeper penetration of the air. This configuration also gave sufficiently enough residence time required for the oxidation of PAH.

One of the major requirements of the combustion chamber is the outer casing temperature of the combustion chamber should be order of 100-150°C. This can be achieved via two ways, first by providing insulating layers on the combustion chamber and second by passing a coolant fluid on the walls of the combustion chamber. The second alternative is quite complicated at this stage and therefore first alternative was chosen for further study. Parameters such as thermal shocks, thermal gradients, structural properties, thermal conductivity of insulating material were considered while selecting the insulating material. The combustion chamber was designed using three different insulating layers. Thickness of each layer of insulating material was estimated based on temperature gradient requirements. For estimating the insulating thickness initially an engineering approach was used (see Equation 1).

$$R = \frac{1}{2\pi h_i r_1} + \sum_{k=1}^{n-1} \frac{\ln\left(\frac{r^{(k+1)}}{r_k}\right)}{2\pi \lambda_k} + \frac{1}{2\pi h_e r_n} \quad (1)$$

A final check on the effect of insulating materials on the heat distribution was carried out using CFD. Any discrepancy between the estimated insulating layer thickness using engineering model and CFD was adjusted in the final design of the combustion chamber.

Controlling the outer layer temperature only with insulating material is a challenge due to non-linear behavior of insulation thickness on the temperature drop through insulating layers. The study indicated that the effect of insulation thickness and insulating material properties on the temperature drop is non-linear and beyond certain insulation thickness the temperature of the outer shell does not reduce significantly. On the other hand, the outer diameter and weight of the combustion chamber should not exceed the critical values. The outer diameter of the combustion chamber was fixed at 650 mm. Controlling the outer temperature with insulating material alone was not sufficient and therefore extended surfaces (Fins) were provided to achieve the higher heat transfer rates. The fin was very useful in controlling the outer wall temperature.

After going through many iterations the final design and size of the combustion chamber was proposed and shown in Figure 3. CFD simulations of the final configuration was performed and presented in following sections. The CFD results of intermediate design is not presented here and it is beyond the scope of the paper.

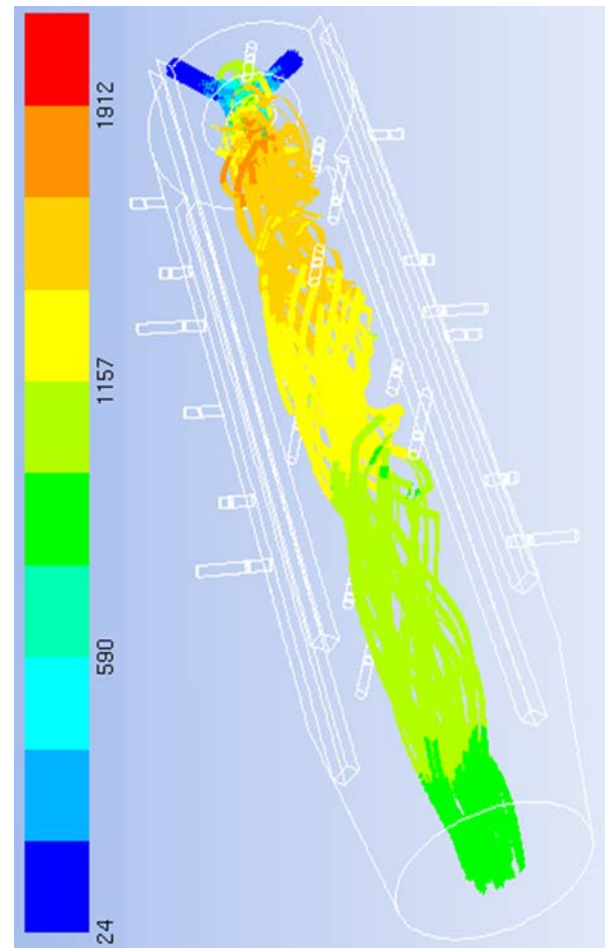


Figure 5: Pathlines coloured with gas temperature (°C)

## RESULTS AND DISCUSSIONS

A maximum velocity at the outlet of the chamber is around 4 m/s. The first and third stations had offset for secondary air injection (see Figure 3 and Figure 8/9), but second and fourth air injections were perpendicular to the chamber (see Figure 10/11). The second and fourth station of secondary air injection is supplying air normal to the combustion chamber to achieve a deeper penetration of the air. The penetrated air interacts strongly with process gas and thus helps in better combustion of the process gases. The converging section of the combustion chamber close to the outlet makes flow streamline along the wall of the combustion chamber. The flow inside the combustion chamber is somewhat complicated due to offset supply of air (see Figure 5). The pathlines from the fuel inlet is shown in Figure 5. The pathlines are colored with gas temperature. Highest temperature is nearly 1900 °C. A circulating pattern of the gas stream can be seen in the Figure 5. The gas released from the co-axial fuel/air inlet is along the direction of the combustion chamber, the gas undergoes to a circulation flow pattern when it meets the secondary air released from the offset injection (first stations of secondary air inlet). This circulating pattern helps in increasing the residence time of the PAH gas components. It can also be observed that the temperature of the gas stream is never less than 850°C, which ensure a possibility of having the complete combustion of PAH.

The maximum temperature is also not more than 1950 °C which is very helpful for not allowing the substantial NOx. Formation. There are mainly three routes for NOx formation; 1) thermal NOx, 2) fuel NOx, and 3) prompt Nox, among them the rate of thermal NOx formation exponentially varies with the gas temperature and for every increase in 90 degree the rate of NOx formation doubles at temperature above 1927 °C .

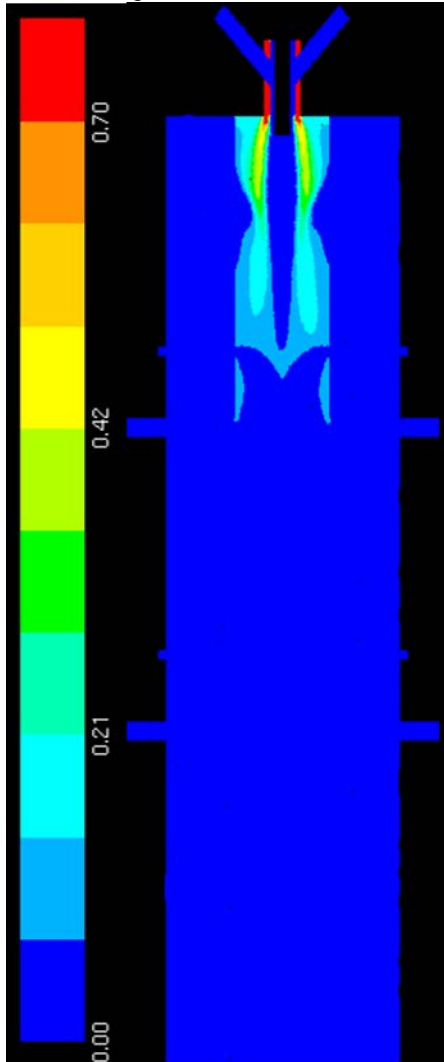


Figure 6: CO mass fraction in the central plane

CO in the middle plane of the combustion chamber is illustrated in Figure 6. It can be seen that the most of the CO is consumed before the second station for secondary air injection. However, increasing the secondary air injection velocity beyond optimum at injection perpendicular to the combustion chamber might lead to the some challenges.

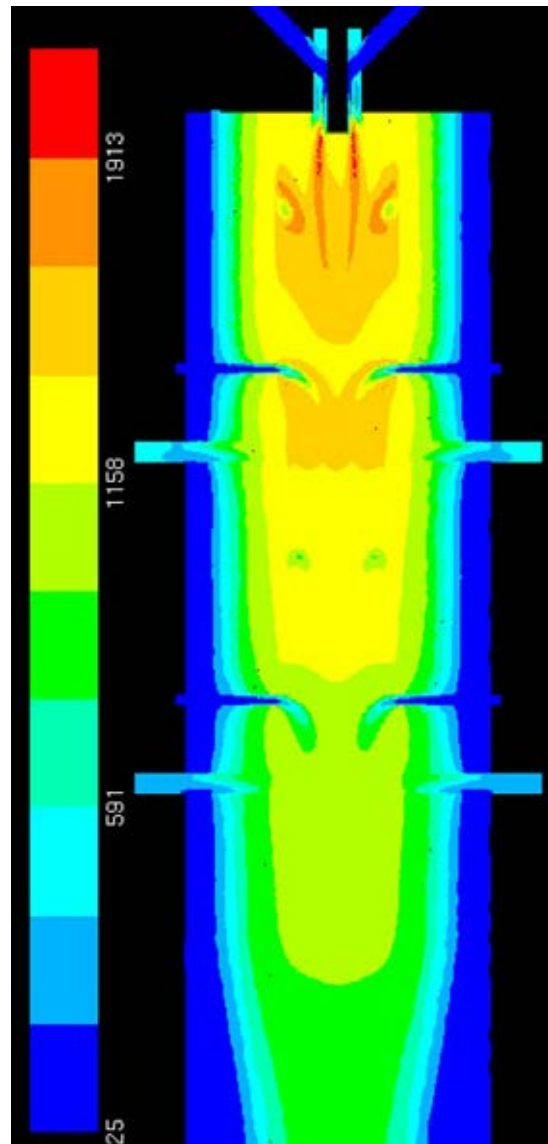


Figure 7: Temperature distribution in the central plane (°C)

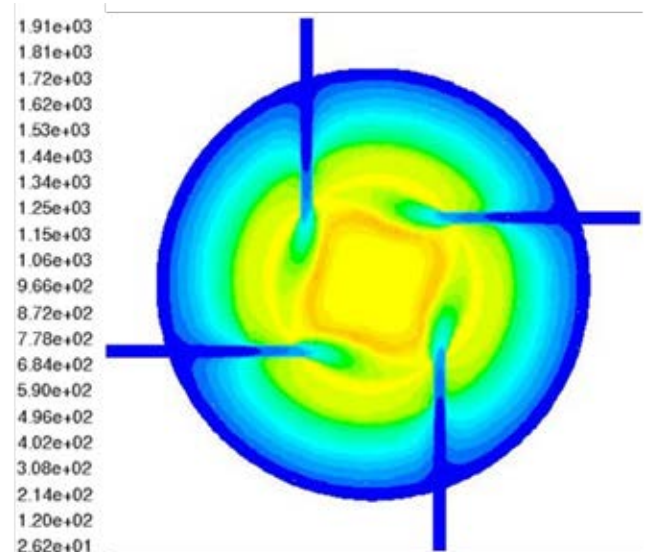


Figure 8: Temperature distribution at first station of secondary air injection

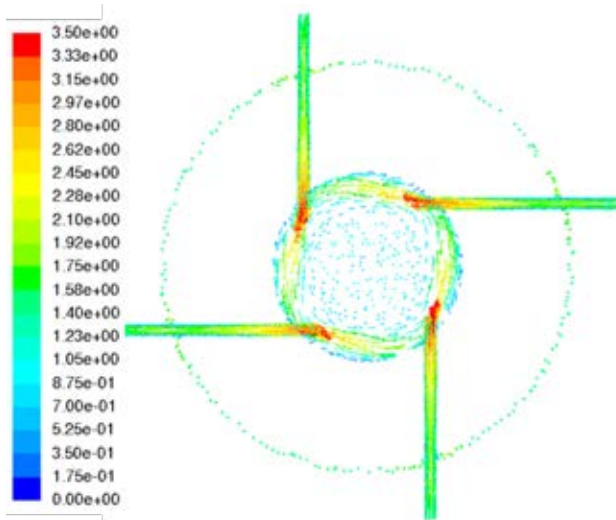


Figure 9: Velocity vector colored by velocity magnitude (m/s) at the first station

Temperature distribution in the central plane is shown in Figure 7. The highest temperature of gas is around 1950 °C and the outlet temperature of the gas is around 850 °C. The peak temperature occurs close to the lab burner region, in this region fuel and oxidizer reacts and develops a stabilized flame. The temperature distribution of the combustion chamber section at first secondary air inlet is shown in Figure 8. A flame (squared shape high temperature zone) is visible at a location where fresh air from the secondary air inlet interacts with gas coming from co-axial fuel and air inlets. In the same location, velocity distribution is shown in Figure 9. The velocity distribution shows two distinct pattern first one is recirculating pattern due to secondary air injection and the second zone is due to co-axial flow. The temperature and velocity distributions are completely different at the second station for secondary air injection (see Figure 10 and Figure 11). The circulation pattern around the secondary air injection is not visible anymore and air is penetrating deeper inside the combustion chamber.

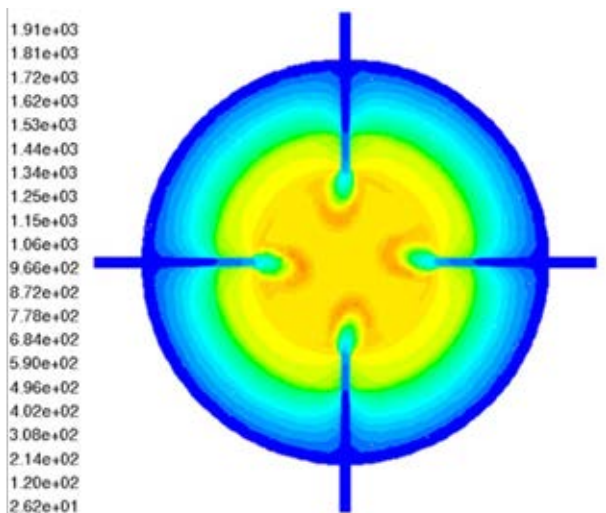


Figure 10: Temperature distribution at second station of secondary air injection

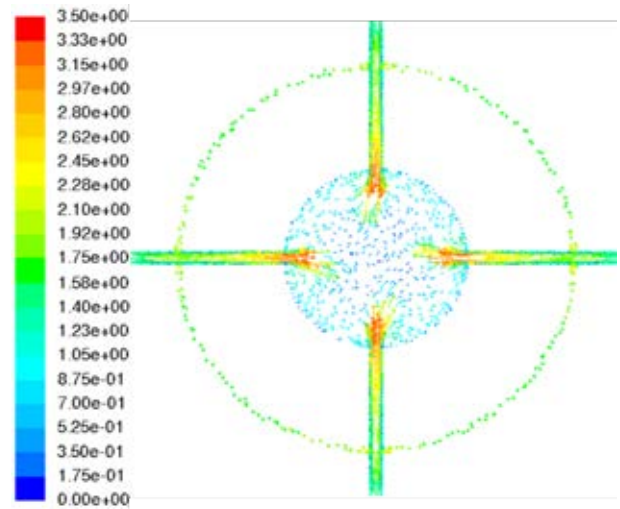


Figure 11: Velocity vector colored by velocity magnitude at the second station

## CONCLUSION

The design concept of combustion chamber for combusting the process gas obtained during the SAF reduction process has been presented. Design principle of the proposed combustion chamber is different from the traditional jet engine combustion chamber and boiler/furnace combustion chamber. New design principle of combustion chamber has been presented for scaling the combustion chamber design. The major parameter such as residence time and maximum/average temperature of the process gas, outer diameter and outer shell temperature of chamber and power of the combustion chamber are considered while designing the combustion chamber. CFD studies have shown that the secondary air injection is necessary for minimization of NO<sub>x</sub> formation. The secondary air injection also increases the residence time of the process gas while maintaining a uniform temperature inside the chamber, which is required for an efficient combustion of the PAH. The proposed combustion chamber gave an average residence time of 2s and an average temperature of around 800 °C suitable for PAH oxidation.

## ACKNOWLEDGMENT

The research work carried out in this article is funded by SCORE (Staged Combustion for Energy Recovery in Ferroalloy industry) project funded by Norwegian research council and The Norwegian Ferroalloy Producers Research Association (Ferrolegeringsindustriens Forskningsforening (FFF)). Funding from the SCORE project is greatly acknowledged

## REFERENCES

- ANSYS, INC. 2016. *ANSYS FLUENT Theory Guide*.
- Drake, Michael C., and Richard J. Blint. 1988. 'Structure of Laminar Opposed-flow Diffusion Flames With CO/H<sub>2</sub>/N<sub>2</sub> Fuel', *Combustion Science and Technology*, 61: 187-224.
- Heimir Hjartarson, Halldor Palsson, and Gudrun Saevarsdottir. 2010. "Waste Heat Utilization From A Submerged

- Arc Furnace Producing Ferrosilicon." In *The Twelfth International Ferroalloys Congress Sustainable Future*. Helsinki, Finland: INFACON.
- Kamfjord, N.E., E. H. Myrhaug, H Tveit, and Wittgens B. 2010. "Energy Balance Of A 45 Mw (Ferro-) Silicon Submerged Arc Furnace." In *The Twelfth International Ferroalloys Congress Sustainable Future*. Helsinki, Finland: INFACON.
- Mati, Karim, Alain Ristori, GaËlle Pengloan, and Philippe Dagaut. 2007. 'Oxidation of 1-Methylnaphthalene at 1–13 atm: Experimental Study in a JSR and Detailed Chemical Kinetic Modeling', *Combustion Science and Technology*, 179: 1261-85.
- Schei, A., J. K. Tuset, and H. Tveit. 1997. *Production of High Silicon Alloys* (Tapir).